Model of thermally activated magnetization reversal in thin films of amorphous rare-earth–transition-metal alloys

A. Lyberatos, J. Earl, and R. W. Chantrell
Department of Physics, Keele University, Keele, ST5 5BG, United Kingdom
(Received 31 July 1995)

Monte Carlo simulations on a two-dimensional lattice of magnetic dipoles have been performed to investigate the magnetic reversal by thermal activation in rare-earth–transition-metal (RE-TM) alloys. Three mechanisms of magnetization reversal were observed: nucleation dominated growth, nucleation followed by the growth of magnetic domains containing no seeds of unreversed magnetization, and nucleation followed by dendritic domain growth by successive branching in the motion of the domain walls. The domain structures are not fractal; however, the fractal dimension of the domain wall was found to be a good measure of the jaggedness of the domain boundary surface during the growth process. The effects of the demagnetizing field on the hysteretic and time-dependent properties of the thin films were studied and some limitations in the application of the Fatuzzo model on magneto-optic media are identified.

I. INTRODUCTION

The magnetization reversal process in amorphous rare-earth–transition-metal (RE-TM) alloys[1] is of considerable practical interest in thermomagnetic recording. Thermal activation is one of the factors that determines the stability of the thermomagnetically grown magnetic domains against collapse or irregularity and is, therefore, of practical relevance in defining the signal-to-noise ratio.[2]

The magnetization reversal in amorphous magneto-optic media occurs in general by a process of nucleation followed by domain growth. The observation of a finite domain-wall coercivity can be interpreted by postulating the existence of nanoscale structural and magnetic inhomogeneities that act as pinning centers.[3] It is possible to study the origin of the coercivity by computer simulations that employ the dynamic Landau-Lifshitz-Gilbert equation of motion for the magnetization in the absence of thermal fluctuations.[3] Such studies have demonstrated that it is important to distinguish the nucleation coercivity H_n, which is determined primarily by fluctuations in the perpendicular anisotropy constant K_u, from the wall-motion coercivity H_w that depends on fluctuations in the exchange stiffness constant and the dispersion in easy axes.[3] These findings are consistent with the experimental observation that the nucleation coercivity can be substantially larger than the wall-motion coercivity in RE-TM alloys, resulting in rectangular hysteresis loops.[4]

When the external field is close to but less than the nucleation coercivity H_n, magnetization reversal is still possible by thermal activation over the local energy barriers. Thermoactivated reversal has been observed in a variety of amorphous RE-TM alloys such as Tb-Fe,[5–10] Tb-Fe-Co,[11–13] Gd-Fe,[14–16] Gd-Tb-Fe,[15,16] and Tb(Co)-based alloys.[16] There is a substantial body of evidence for the presence of a thermal magnetic aftereffect: (1) the observation that the domain-wall motion is not a continuous process but consists of discrete Barkhausen jumps of small sections of the wall.[8] (2) the slow decay of the magnetization under constant external field conditions,[5] and (3) the exponential dependence of the domain-wall velocity on the external applied field.[6,14,15]

The precise form of the time dependence of the magnetization $M(t)$ in a constant field depends on the relative balance of the nucleation and wall-motion processes during magnetic reversal. A theory by Fatuzzo[17] assumes that the nucleated domains are circular with initial radii r_c that grow at a constant velocity v, while the rate of nucleation R remains constant. The theory predicts that the shape of the time-dependence curves $M(t)$ depends on a single parameter $\kappa = v/Rr_c$. From the shape of the experimental curves $M(t)$, approximate values of κ can be determined.[16] Fatuzzo's theory, however, does not account for the presence of a dispersion in energy barriers that may arise, for example, from local fluctuations of the exchange stiffness constant and the uniaxial anisotropy K_u or alternatively from the spatial and temporal variations of the demagnetizing field. A dispersion in energy barriers is necessary to account for the common observation that the nucleated domains are frequently irregular in shape[18,19] and their subsequent growth may be dendritic, forming a fractal structure.[6,8,10]

The stability of the domain shape of cylindrical domains in homogeneous thin films with perpendicular anisotropy but low domain-wall coercivity depends on the wall stiffness,[20] which is determined by the competition between the domain wall and demagnetizing energy.[21] When the demagnetizing energy is relatively large, the stiffness of the domain wall is low and the domain shape is more susceptible to local deformation by pinning sites. Dendritic growth occurs when the stiffness of the wall is sufficiently low so that the growth of the reverse magnetization is dominated by the geometry of the pinning sites.[10] The computation[10] or measurement[18] of the fractal dimension of the boundary surface of the magnetic domains have been suggested as useful methods of characterization of the jaggedness of the domain boundary.

The simulation of thermoactivated magnetic reversal under constant external field conditions can best be carried out using a Monte Carlo algorithm[22] that simulates accurately the kinetic process as in Ref. 23 Kirby *et al.*[24] applied the algorithm on thin films for magneto-optic recording and ob-

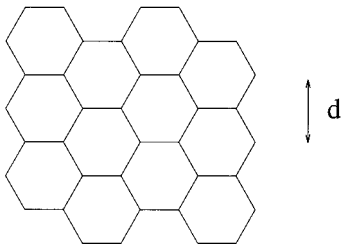

FIG. 1. A schematic illustration of the planar hexagonal array of cells used in the Monte Carlo model.

served two distinct reversal mechanisms in their simulations dependent on the competition between the demagnetizing and domain-wall energy. In the case when the demagnetizing forces are dominant, the reversal occurred by continuous nucleation; otherwise, if the wall energy is relatively large, the reversal occurred by slow nucleation followed by rapid domain growth. The simulation of dendritic domain growth, however, using that model is not possible (as some trial runs have confirmed) because of the imposed condition of the dominance of the wall energy for the observation of domain growth, whereas dendritic growth arises primarily from the local inhomogeneities in the demagnetizing field.[8,10]

A numerical model of the dendritic growth of the reverse magnetization was reported by Sayko *et al.*[10] This model considered the growth of one domain only and did not consider the possibility of other nucleation events. Our objective is to show that to simulate the nucleation process and dendritic domain growth, it is necessary to consider the difference in the intrinsic energy barriers for nucleation and wall motion. For amorphous RE-TM alloys, this approach is consistent with the difference observed between the coercivities of nucleation and domain-wall motion. The numerical model of thermal activation adopted in our work is described in Sec. II and the Monte Carlo algorithm in Sec. III. A modification of the standard algorithm that allows the simulation of the dynamic response of the system during an hysteresis cycle is also presented. In Sec. IV, it is shown that the model simulates all the magnetic reversal mechanisms observed in practice. It is also shown that the domain structures may be porous but are not strictly fractal, since the basic property of scale invariance[25] is not satisfied, i.e., the domain structures do not look the same as the domain size increases. The assumption that dendritic growth results in fractal domain structures[10] does not appear, therefore, to be justified. The perimeter of the domains, however, is shown to be a fractal curve, and its fractal dimension turns out to be a useful figure of merit of the irregularity of the domain growth. An analysis of the numerical data on the hysteretic and time-dependent properties of the films in relation to the Fatuzzo theory is also carried out to determine the effects of the demagnetizing forces in the magnetic reversal.

II. DESCRIPTION OF THE MODEL

The amorphous thin film was modeled by a 512×512 planar hexagonal array of cells that is schematically shown in Fig. 1. The geometry of the system is essentially similar to the model of Kirby *et al.*,[24] although the detailed treatment of thermoactivated reversal is different. The domain wall is assumed to be pinned at the boundary between the cells, which serves to describe the geometry of the ''defects.'' The separation of neighbor cells d is assumed to be much larger than the domain-wall thickness so that any nanoscale features in the domain-wall motion are ignored. This assumption is justified by the experimental observation that the domains walls undergo, by thermal activation, irreversible jumps over a distance $\approx0.5\ \mu$m,[7] whereas the domain-wall thickness is much smaller, for example, of the order ≈10 nm, in Tb-Fe-Co films.[4] At the start of the simulation, the magnetization in each cell is in the $+z$ direction perpendicular to the plane of the film and is allowed to switch to the $-z$ direction along an external applied field H_a. We can, therefore, express the magnetization $\mathbf{M}_i$ at any site i as $\mathbf{M}_i=\epsilon_i M_s\hat{\mathbf{k}}$, where $\epsilon=\pm1$ and $\hat{\mathbf{k}}$ is the unit vector normal to the plane of the film.

The energy density U at a local site i is given by the sum of the anisotropy, Zeeman, demagnetizing, and domain-wall energy densities.

$$U=U_a+U_z+U_d+U_w=\frac{K_u}{M_s^2}\,|\hat{\mathbf{k}}\times\mathbf{M}|^2-\mathbf{M}_i\cdot\mathbf{H}_a$$
$$-\mathbf{M}_i\left(\sum_{j\neq i}D_{ij}\mathbf{M}_j+\tfrac{1}{2}D_{ii}\mathbf{M}_i\right)$$
$$+\frac{1}{2}\left(n-\frac{\mathbf{M}_i\cdot\Sigma_{j=1}^{n}\mathbf{M}_j}{M_s^2}\right)\frac{E_w}{V},\qquad(1)$$

where H_a is positive along the z direction, D_{ij} are the scalar components of the demagnetization matrix, $n=6$ is the number of neighbor cells, E_w is the wall energy in the interface between two cells, and V is the volume of a cell. Note that the uniaxial anisotropy energy density including the self-demagnetizing term $(K_u/M_s^2)|\hat{\mathbf{k}}\times\mathbf{M}|^2-(1/2)D_{ii}M_s^2$ in Eq. (1) is a constant term, since the magnetization is confined at equilibrium along the easy axis $\hat{\mathbf{k}}$. Ultimately, we are interested in thermal activation over intrinsic energy barriers to which the local anisotropy makes an important contribution.

The local field $\mathbf{H}_{l,i}$ on the ith cell that is effective during the thermal activation is given from

$$\mathbf{H}_{l,i}=-\frac{\Delta U}{\Delta\mathbf{M}_i},\qquad(2)$$

where $\Delta\mathbf{M}_i$ is the net change of the magnetization arising from the thermoactivated reversal. The local field, as defined by Eq. (2), is different from the effective field $\mathbf{H}_{\mathrm{eff},i}=-\partial U/\mathbf{M}_i$ used in micromagnetic computations that also incorporates a contribution from the local anisotropy. Using Eq. (1), the local field is given by

$$\mathbf{H}_{l,i}=\mathbf{H}_a+\sum_{j\neq i}D_{ij}\mathbf{M}_j+\frac{E_w}{2VM_s^2}\sum_{j=1}^{n}\mathbf{M}_j.\qquad(3)$$

The activation energies of nucleation $E_{b,n}$ and wall motion $E_{b,w}$ are assumed to be linearly dependent on the local field.

$$E_{b,n,i}=E_{b,n}^0+V_{\mathrm{act}}\mathbf{M}_i\cdot\mathbf{H}_{l,i},\qquad(4)$$

$$E_{b,w,i}=E^0_{b,w}+V_{\rm act}\mathbf{M}_i\cdot\mathbf{H}_{l,i}, \tag{5}$$

where $V_{\rm act}$ is the activation volume (assuming strong domain wall pinning) and $E^0_{b,n}, E^0_{b,w}$ are the intrinsic energy barriers that are related, and have similar origin, to the coercivities of nucleation H_n and wall-motion H_w, respectively. The activation energy of a cell is evaluated using Eq. (4) if none of the neighbor cells has reversed magnetically; otherwise Eq. (5) is employed.

The field dependence of the energy barrier is dependent on the detailed activation mechanism and is not known in detail. For films of relatively square hysteresis, the change in field during magnetic reversal is small so the linear approximation adopted in Eqs. (4) and (5) appears to be plausible. The assumption of a linear dependence of the energy barriers on the external field is supported by direct experimental evidence[7] in the case of thermoactivated domain-wall motion. It is also supported from the observation that both the rate of nucleation R and the domain wall velocity v are exponentially dependent on the external field H_a (Refs. 7, 8, 15, 16, 26, and 27). The fluctuation field $H_f=kT/(\partial E_b/\partial H_a)$ is also found to remain essentially constant during the magnetization process[13] and to be independent of the applied field.[13,28] For films of sheared hysteresis, the field dependence of the energy barrier may be nonlinear; however, the linear approximation does not invoke an error in the study of the domain structures but only on the time scale of magnetic reversal.

The activation volume $V_{\rm act}$, for strong or weak domain-wall pinning in one dimension, is the volume associated with the change in magnetization between the maximum and minimum energy positions of the domain wall.[29] This volume is smaller but not simply related to the volume between the pinning centers, i.e., between two minimum-energy positions. In the case of thermoactivated nucleation and motion of nonplanar walls, the energy surface may be more complex; however, the physical meaning of the activation volume is probably similar, provided the maximum is replaced by a saddle point.[30] The nucleation of magnetization reversal may therefore start in a small region within a cell at which point the saddle point in the energy surface is reached. This is then followed by the irreversible expansion of the original nucleus to fill the entire cell. The activation volume is, therefore, expected to be smaller than the size of the hexagonal cells that defines the separation between the pinning centers in our model ($V_{\rm act}<V$). Measurements carried out on ultrathin ferromagnetic films for magneto-optic recording[31] confirm that $V_{\rm act}$ is smaller than the volume V between the pinning centers.

Here, it is assumed that the activation volumes for thermoactivated nucleation and wall motion are identical, although there is no clear physical reason that this should be the case. The simplification is carried out, since there is experimental evidence[16] from time-dependence measurements in GdFe and GdTbFe alloys that the activation volumes for nucleation and wall propagation are not substantially different. The evidence is manifested indirectly in the invariance in the shape of the $M(t)$ curves when measured at different fields. The shape of the curves depends on Fatuzzo's parameter $\kappa=v/Rr_c$, which is related to the difference in the activation volumes. Direct evaluation of the activation volumes from the exponential dependence of v,R on the field H_a for GdFe and GdTbFe alloys leads essentially to the same conclusion.[16]

The activation energies for both nucleation and wall propagation at a local site i are obtained by substitution of Eq. (3) into Eqs. (4) and (5):

$$E_{b,nw,i}=E^0_{b,nw}+V_{\rm act}\mathbf{M}_i\cdot\left(\mathbf{H}_a+\sum_{j\neq i}D_{ij}\mathbf{M}_j+\frac{E_w}{2VM_s^2}\sum_{j=1}^{n}\mathbf{M}_j\right). \tag{6}$$

The elements of the demagnetization matrix were evaluated using a dipole approximation $D_{ij}=-V/r^3_{ij}$ for a 6×6 array of neighbor cells, using periodic boundary conditions to extend the Monte Carlo array and a mean-field approximation for the contribution of more distant cells. The separation r_{ij} of the cells i,j can be expressed in terms of the coordinates (l,m) with respect to the hexagonal Bravais lattice:

$$r_{ij}=d\sqrt{(l_i-l_j)^2+(m_i-m_j)^2+(l_i-l_j)(m_i-m_j)}. \tag{7}$$

The dipole approximation overestimates the demagnetizing energy, and the error is largest for nearest-neighbor interactions (for instance it was estimated as 17% for a cubic lattice[32]). This error can be tolerated here, since we are interested only in a qualitative description of the results of the simulations.

III. THE MONTE CARLO ALGORITHM

At the saturation remanence the mean demagnetizing field is of the order $H_d=-N_sM_{r,s}$,[20] where N_s is the sheet demagnetization factor. The demagnetizing field is assumed to be of insufficient strength to initiate a nucleation process. Since the magnetization in the model is confined along the normal to the film surface, no reversible magnetization changes can be considered, and the squareness ratio $M_{r,s}/M_s=1$. Irreversible, thermally activated transitions, therefore, only occur when the applied field has a direction opposite to the direction of the magnetization. For this reason, the probability r_i per unit time of thermal activation at a local site i has been taken as

$$r_i=\begin{cases} f_0e^{-E_{b,i}/kT}, & \text{if } \mathbf{M}_i\cdot\mathbf{H}_a<0 \\ 0, & \text{if } \mathbf{M}_i\cdot\mathbf{H}_a>0, \end{cases} \tag{8}$$

i.e., the probability of activation against the applied field is ignored. f_0 is a frequency factor of the order 10^{-9}–10^{-12} $\sec^{-1}$.[33,34] The rate for the entire system to evolve is $R=\Sigma_i r_i$. The probability that no change of state has occurred at time t is

$$p(t)=e^{-Rt}. \tag{9}$$

In the case when magnetic reversal is dominated by domain-wall motion, we expect that $r_i<r=\max(r_i)$ for most cells i. It is, therefore, of advantage to employ the following Monte Carlo algorithm.[22]

(1) Initialize the time $t=0$.
(2) We consider t as a random variable, which is generated according to the distribution $p(t)$ above, for example, by setting $t=-\ln\xi/R$, where $0<\xi<1$ is a random number.

(3) A cell ν is selected with probability r_ν/R and is allowed to reverse magnetically. The selection can be carried out by evaluating the sum $S_\nu=\Sigma_{i=1}^{\nu} r_i/R$ for increasing ν until $S_\nu>\xi$, where $0<\xi<1$ is a random number.

This algorithm assumes that the rate R remains constant until a change of state occurs. This assumption is valid provided that the external field is constant in magnitude. When simulating an hysteresis loop, however, the external field H_a is linearly dependent on time,

$$H_a(t)=H_a(0)-\frac{dH_a}{dt}\,t. \tag{10}$$

During the course of an average time step $\Delta t=1/R$ that elapses until the first change of state occurs, the rate R will have changed in magnitude so that the use of the initial value $R_0=R(t=0)$ will involve an error. Using Eqs. (4), (5), and (10), the rate r_i in Eq. (8) for those moments that have not switched yet along the direction of the applied field can be expressed as

$$r_i=r_{0,i}e^{\beta t}, \tag{11}$$

where

$$r_{0,i}=f_0 e^{-E_{b,i}(t=0)/kT}, \tag{12}$$

$$\beta=\frac{M_s V_{\rm act}}{kT}\frac{dH_a}{dt}. \tag{13}$$

The total rate R also increases exponentially with time.

$$R=\sum_i r_i=\sum_i r_{0,i}e^{\beta t}=R_0 e^{\beta t}. \tag{14}$$

The probability that no change has occurred at time t is

$$p(t)=\exp\left(-\int_0^t R(t)dt\right),$$

$$=\exp\left(-\frac{R_0}{\beta}[e^{\beta t}-1]\right). \tag{15}$$

The simulation of kinetic effects during an hysteresis cycle can be carried out using the algorithm that was described above; however, on the second step of that algorithm the time t is now generated at random from the distribution given by Eq. (15), using the following expression:

$$t=\frac{1}{\beta}\ln\left(1-\frac{\beta\,\ln(\xi)}{R_0}\right), \tag{16}$$

where $0<\xi<1$ is a random number. An advantage in using Eq. (16) is that the time interval and associated external field when the first nucleation occurs can be evaluated in one step. The alternative method of approximating the continuous variation of the external field by a sequence of small steps is not as computationally efficient.

An analytic expression for the expectation value of the nucleation coercivity of the thin film can be obtained by replacing $-\ln(\xi)$ by the average value 1 in Eq. (16). The mean time that elapses when the first nucleation occurs is

$$\langle t\rangle=\frac{1}{\beta}\ln\left(1+\frac{\beta}{R_0}\right). \tag{17}$$

The time dependence of the energy barrier of nucleation is given by

$$E_{b,n}(t)=E_{b,n}(0)-M_s V_{\rm act}\frac{dH_a}{dt}\,t=E_{b,n}(0)-kT\beta t. \tag{18}$$

Using $R_0=Nf_0\exp[-E_{b,n}(0)/kT]$, where N is the total number of nucleation sites (in our model the number of hexagonal cells) and assuming that $\beta/R_0\gg 1$, the expectation value of the energy barrier when the first nucleation occurs is given by

$$\frac{E_{b,n}(\langle t\rangle)}{kT}=\frac{E^0_{b,n}}{kT}-\ln\left(\frac{\beta}{R_0}\right)=\ln\left(\frac{Nf_0}{\beta}\right), \tag{19}$$

which is valid for $Nf_0/\beta>1$. The expectation value of the nucleation field H_n at a given temperature can be obtained from Eqs. (3), (4), and (19),

$$H_n(T)=H_n(0)-H_f\ln\left(\frac{Nf_0}{\beta}\right), \tag{20}$$

where $H_f=kT/(M_s V_{\rm act})$ is the fluctuation field. The nucleation coercivity is linearly dependent on the logarithm of the rate of change of the applied field and of the number N of nucleation sites but does not depend on the initial value of the applied field.

The results of the Monte Carlo simulations are dependent on $\beta=d(H_a/H_f)/dt$ and on the dimensionless parameters $w=V_{\rm act}E_w/(2VkT)=E_w/(2M_sVH_f)$, $z=V_{\rm act}VM_s^2/(kTd^3)=H_{\rm dip}/H_f$, and $k=\exp[(E^0_{b,n}-E^0_{b,w})/kT]$, where $H_{\rm dip}=M_sV/d^3$ is the strength of the dipole field at neighbor sites. For constant k, the precise choice of the intrinsic energy barrier $E^0_{b,n}$ (or $E^0_{b,w}$) does not change the shape of the curves $M(t)$ but results only in the scaling of the time according to the relation $M(E^0_{b,n},t)=M(E'^0_{b,n},t\exp[(E^0_{b,n}-E'^0_{b,n})/kT])$. A value $\beta=2\ \sec^{-1}$ was used in the simulations of hysteresis. This value is consistent, for example, with a fluctuation field $H_f\approx 100$ Oe, as observed in TbFeCo alloys[13] and the reduction of the applied field from a saturating value $H_s=5$ to -5 kOe in 50 sec.

IV. RESULTS

Following a presentation of the domain structures and hysteresis loops observed in the simulations, the theory of fractals is employed to characterize the regularity of domain growth and a study of the time dependence of the magnetization under a constant external field is carried out. The conditions that are necessary for the observation of different types of magnetic reversal were first determined. An example of the domain structures that are observed in the simulations is shown in Fig. 2(a). These were obtained using a value $z=2$ for the constant z, which is a measure of the strength of the demagnetizing field and a range of values for the parameters k,w. The magnetic reversal occurs, in general, by a process of nucleation followed by domain growth; however, the extreme cases of nucleation-dominated and wall-motion

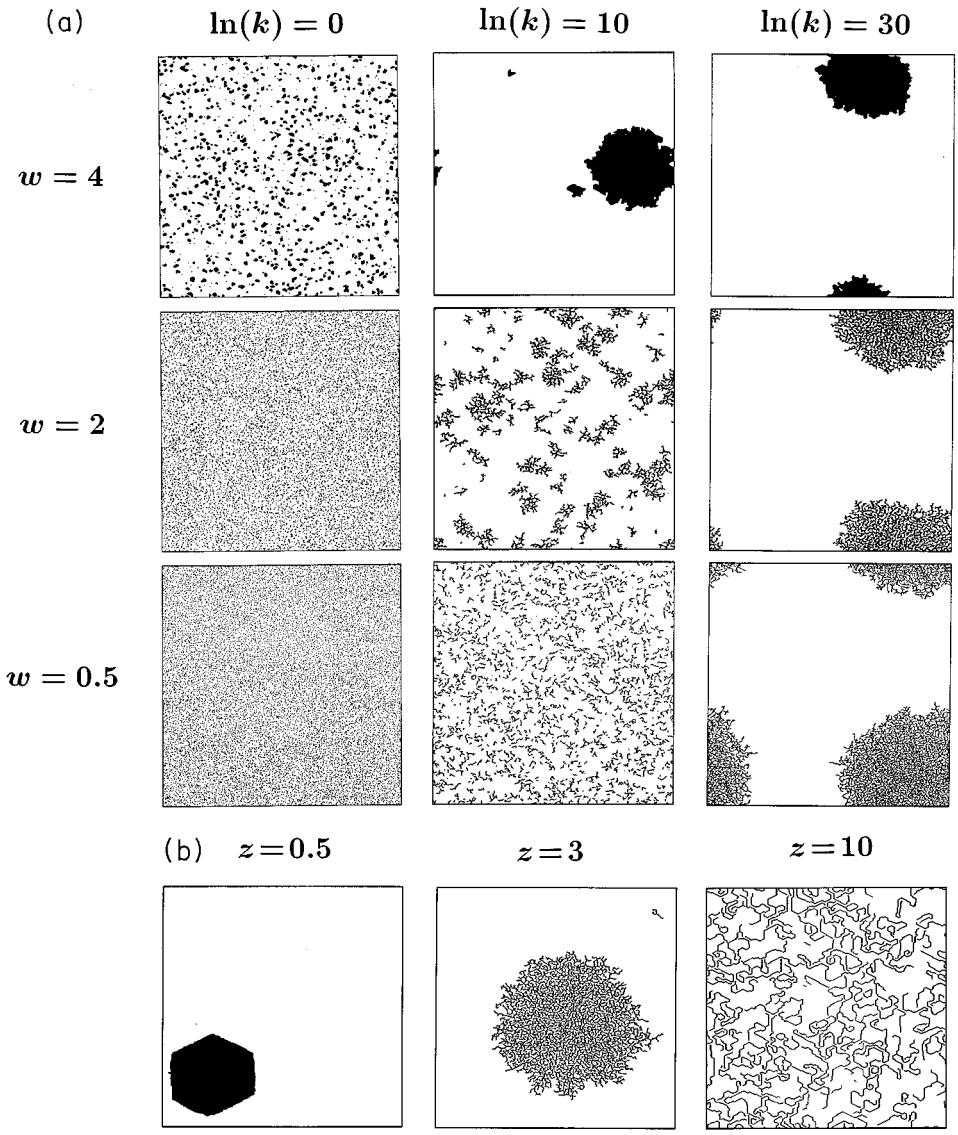

FIG. 2. (a) Domain structures at an early stage during the reversal process ($M/M_s=0.9$) obtained using a value $z=2$ for the constant that is a measure of the strength of the demagnetizing field. (b) Domain structures for different strengths z of the demagnetizing field: $\ln(k)=30$, and $w=2$.

dominated reversal are also observed. The domain boundary is, in general, jagged, and dendritic domain growth is also observed by the branching in the domain-wall motion and the formation of regions of unreversed magnetization in the interior of the domain.

The magnetic reversal is dominated by continuous nucleation when the intrinsic energy barrier of nucleation $E^0_{b,n}$ is not larger that the barrier of wall motion $E^0_{b,w}$, i.e., when the condition $k \leqslant 1$ is satisfied. An additional condition is that the demagnetizing strength z is large in comparison to the wall energy w. In any other case, the magnetic reversal is determined primarily from the domain-wall motion. These results are consistent with the theory of Fatuzzo.[17] According to Fatuzzo's theory, the balance of thermoactivated nucleation and wall motion is determined by a single parameter $\kappa = v/(Rr_c) \propto \exp[(E_{b,n}-E_{b,w})/kT]$, which is proportional to the parameter $k=\exp[(E^0_{b,n}-E^0_{b,w})/kT]$ in our model. An increase in the value of k results in the reduction of the number of nucleated domains, as is shown in Fig. 2(a). In the case when $k=1$ (that was also considered in Ref. 24), reversal dominated by wall motion is still possible when w is large [Fig. 2(a)]. The reason is that the energy barrier of wall motion $E_{b,w}$ is lowered in the vicinity of a nucleated domain by the contribution of the wall energy to the activation process [described by the local-field approximation in Eq. (6)], and the condition $\kappa > 1$ in Fatuzzo's theory is satisfied. The demagnetizing energy instead results in a local enhancement of the barrier $E_{b,w}$ (since the demagnetizing field is smaller than the mean value at the boundary surface of a nucleated domain) and promotes reversal dominated by continuous nucleation.

Figure 2(b) shows domain structures for different demagnetizing strength z. When the demagnetizing strength is sufficiently low, the domain boundary becomes smooth; however, the domains are not cylindrical, and their shape is determined by the hexagonal geometry assumed for the distribution of pinning sites.

We next consider the information on the magnetic reversal that can be provided from the hysteresis loops of the system. The transition of the magnetization as the reverse field is increased is shown in Figs. 3(a) and 3(b) and is obtained using $\ln(k)=0,30$, respectively. When the strength of the demagnetizing forces is enhanced by increasing the value of z, the nucleation coercivity, as expected, is reduced in magnitude. By comparison of the hysteresis loops with domain images, it is possible to determine that the magnetiza-

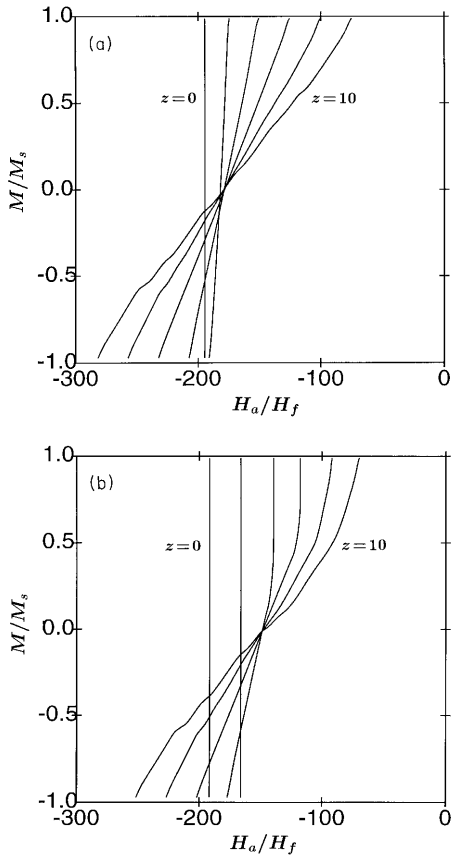

FIG. 3. The hysteretic behavior obtained using in (a) $w=4$, $\ln(k)=0$ and in (b) $\ln(k)=30$ and a range of values $z=0,2,4,6,8,10$ for the constant of demagnetizing strength.

tion reversal in all cases consists of some or all of the following stages.

(1) A spontaneous magnetization jump, arises when the first nucleation is followed by rapid thermoactivated domain growth. The jump is observed when there is a finite difference in the energy barriers $E_{b,n}, E_{b,w}$, for instance, for low values of z and large values of k. In the case when no branching is observed in the domain growth, the hysteresis loops are perfectly rectangular, for instance, when $z=2$ in Fig. 3(b). Since the wall energy has the effect of reducing the barrier $E_{b,w}$ gradually during the reversal process, it is clear that any shearing, in the absence of a dispersion in the intrinsic barriers $E^0_{b,n}, E^0_{b,w}$, in our model must necessarily be attributed to demagnetization forces, as is discussed below.

(2) A linear shearing of a gradient of the order $1/N_s$ may occur as a result of the mean demagnetizing field $H_d=-N_sM$, where $N_s\approx 4\pi$ is of the order of the sheet demagnetization factor but is also dependent on the presence of the domain walls. An approximately linear shearing is observed, for example, in the case of continuous nucleation in Fig. 3(a) but also in the initial stage of magnetic reversal when $z=10$ in Fig. 3(b). The numerical data are consistent with the model of Kooy and Enz,[35] which predicts that the inclusion of the domain structure in the demagnetizing energy leads to steeper hysteresis loops. The model of Kooy and Enz[35] assumes zero domain-wall coercivity and remanence, so the consideration of finite distinct coercivities for nucleation and domain-wall pinning does not appear to modify the effect of the demagnetizing forces on the shape of the hysteresis loop substantially. An approximate expression for the magnitude of the magnetization jump $\Delta M/M_s$ before the shearing occurs can be obtained as follows. First, the energy barriers are expressed to first order as a function of the mean demagnetizing field:

$$E_{b,n}=E^0_{b,n}+M_sV_{\rm act}(H_a-D_sM), \tag{21}$$

$$E_{b,w}=E^0_{b,w}+M_sV_{\rm act}(H_a-D_sM). \tag{22}$$

The first nucleation process occurs when $M=M_s$, and the expectation value of the ratio $E_{b,n}/kT=\ln(Nf_0/\beta)$ [Eq. (19)]. The reduction of the mean demagnetizing field throughout the entire growth process does not modify in this approximation the balance between the rate of nucleation and domain-wall motion (i.e., $E_{b,n}-E_{b,w}$) but reduces the probability of domain-wall motion (i.e., $E_{b,w}$). It is reasonable to assume that the thermoactivated domain-wall motion is terminated under a similar condition, i.e., when $E_{b,w}/kT\approx\ln(Nf_0/\beta)$, and subtracting Eq. (22) from Eq. (21) results in an expression for the magnetization jump of the form

$$\frac{\Delta M}{M_s}=\frac{E^0_{b,n}-E^0_{b,w}}{D_sM_s^2V_{\rm act}}=\frac{H_n-H_w}{H_{d,s}}\propto\frac{\ln(k)}{z}. \tag{23}$$

H_n, H_w are here defined as the coercive fields of nucleation and domain-wall motion (for a fixed value of the magnetization) that make the respective energy barriers vanish, and $H_{d,s}=N_dM_s$ is the mean demagnetizing field at saturation. In the case of continuous nucleation ($E^0_{b,n}=E^0_{b,w}$), $\ln(k)=0$, and there is no jump, so that the hysteresis loop is sheared during the entire reversal process. The limitations of the model restrict, in practice, the usefulness of Eq. (23); for example, it cannot be applied to systems characterized by a dispersion in energy barriers, i.e., a dispersion in coercivities of nucleation and domain-wall motion. Furthermore, if the jump size predicted by Eq. (23) is large, it is likely that the shearing of the hysteresis occurs by a different mechanism, as is discussed below.

(3) When no more space is available for domain expansion in any direction, i.e., beyond the stage when the domains appear to coalesce, the reversal process is impeded by a substantial reduction in the mean demagnetizing field and the associated enhancement of the barrier of wall motion resulting in shearing of the hysteresis loop. The local magnetic environment at the domain boundary surface that determines the rate of thermoactivated growth is nontrivially modified. The onset of this type of shearing occurs, for instance, in Fig. 3(b), when $M/M_s=0.1$ for $z=4$ and $M/M_s=0.5$ for $z=10$. The size of the regions of unreversed magnetization in the maze-type domain structure increases with demagnetizing strength z [Fig. 2(b)], and consequently the onset of this type of shearing occurs (for large z) at larger values of the magnetization.

Similar sheared hysteresis loops have been observed in

Tb/Fe (Ref. 36) and Pt/Co (Ref. 37) multilayers. The shearing is only observed for films of relatively large thickness h, where the demagnetizing field strength $z \propto h/d$ is strong. For Pt/Co multilayers of large thickness, an enhancement of the shearing close to the coercive point has been reported, and direct domain observations in this case indicate that the domain growth is irregular with no evidence of uniform expansion. It was suggested that the non-uniform expansion may be controlled by defects,[37] i.e., the physical microstructure of the Co/Pt films of different thickness may be different. The Monte Carlo simulations indicate that this type of shearing can occur as a result of the dendritic growth of the magnetization, by simply increasing the demagnetizing strength (not the distribution of defects). Since there is no evidence that the defect structures are dependent on the thickness of the films,[38] the irregular domain growth in thick films should be attributed not only on the presence of defects but also on micromagnetic considerations.

The regularity of the domain growth has been characterized using the theory of fractals. Fractal patterns possess the property of scale invariance.[39] All physical systems, however, have a characteristic smallest length scale. In the present model, the smallest length is imposed by the finite size of the cells of the two-dimensional array. For this reason, an appropriate fractal measure is the cluster or mass fractal dimension D_m.[40] To define the mass dimension, we consider connected cells that have reversed magnetically as forming clusters and use the number-radius relation[40]

$$N(r) = N_0 \left(\frac{r}{R_g} \right)^{D_m} f\left(\frac{r}{R_g} \right), \tag{24}$$

where N_0 is the total number of cells in a cluster and $N(r)$ is the number of cells within a radius r from the nucleation site. The crossover function $f(x)$ is constant for $x<1$ and tends to x^{-D_m} for $x>1$ so that $N(r) \rightarrow N_0$ for $r \gg R_g$. R_g is the radius of gyration defined from

$$R_g = \sqrt{\sum_i^{N_0} r_i^2 \Big/ N_0}, \tag{25}$$

where r_i is the separation of the ith cell from the nucleation site. The mass dimension D_m $(1 \leqslant D_m \leqslant 2)$ for a given domain at some stage during the growth process is evaluated from the slope of the straight line obtained by plotting $\ln[N(r)]$ as a function of $\ln[r/R_g]$, as shown in Fig. 4(a). A linear relationship is obtained for $r/R_g < 1$, where the effect of the crossover function $f(r/R_g)$ can be ignored. For those domains that exhibit dendritic growth, the mass dimension D_m increases during the growth process. The increase is shown in Fig. 4(b), where D_m averaged over an ensemble of domains is shown as a function of the radius of gyration R_g for different values of z. The increase results from the finite probability of magnetic reversal in the interior of the domain during the growth process of regions that remained initially unreversed. Fractal clusters must satisfy the number-radius relation[40]

$$N = \rho (R/R_0)^{D_m} \tag{26}$$

for a noninteger D_m. Here N is the number of monomers, i.e., the cells, that constitute a cluster, R_0 is the monomer size, R is the radius of the smallest circle containing the cluster, and the density ρ depends on how the monomers are packed. The number-radius relation given by [Eq. (26)] is clearly not satisfied for the domain clusters for a unique D_m during the growth process. The magnetic domains are, therefore, porous but are not strictly fractal, since the fundamental property of scale invariance is not satisfied.

The dependence of the mass dimension D_m on the constant z that is a measure of the strength of the demagnetizing field is shown in more detail in Fig. 4(c). When the demagnetizing field is strong, the observed reduction of the mass dimension D_m is consistent with previous simulations by Sayko *et al.*[10] The presence of a strong demagnetizing field renders the dendritic growth energetically favorable.[8] Here, we present three curves obtained at different stages during the growth process, i.e., different values of the radius of gyration. The curvature can be convex or concave and is sensitive to the precise choice of R_g. The dependence of the dimension D_m on the wall energy constant w is shown in Fig. 4(d). A rather abrupt transition to the maximum value $D_m = 2$ is observed. The sharpness of the transition is attributed on the absence of a dispersion in domain-wall coercivities in the model and the homogeneous magnetic environment of the pores in the interior of the domains. Figures 4(c) and 4(d) represent an example of the competition of the demagnetizing and wall energy in controlling the domain regularity. The variation in the domain structure as the wall energy is enhanced is shown in Fig. 2(a). For example, when $\ln(k) = 30$ and $w = 0.5$, the regions of unreversed magnetization are distributed uniformly within the entire area enclosed by the domain boundary. The uniform distribution probably arises as a result of the absence of a dispersion in intrinsic energy barriers of wall motion in the model. When the wall energy is enhanced $(w = 2)$, the fingers within the domain boundary are thickened uniformly until at some stage $(w = 4)$ the entire area within the domain has reversed magnetically. A similar behavior is observed when the parameter z is varied [Fig. 2(b)]. The variation of domain structure with demagnetizing strength is in good agreement with experimental observation in TbFe films,[7,9] although the observation of a small number of hard pinning sites in the interior of the domains in Co/Pt multilayers[37] and the nonuniform domain collapse in TbFeCo films[19] illustrates the importance of local variations in the domain-wall coercivity.

The fractal dimension of the domain wall $D_w (1 \leqslant D_w \leqslant 2)$ is a useful measure of the jaggedness of the domain boundary. Bernacki and Mansuripur[18] measured the wall dimension in TbFeCo thin films under static conditions using the ruler method[41] and found that repeatable values could be obtained under the same magnification. An alternative method suggested in Ref. 10 is to use the perimeter-area relation[40]

$$\frac{L^{1/D_w}}{\sqrt{A}} = c, \tag{27}$$

where L is the length of the perimeter of a domain and A is the area enclosed by its boundary surface. The constant c is independent of the area A and depends only on the shape of the domain and the length of the ruler used to measure the perimeter.[40]

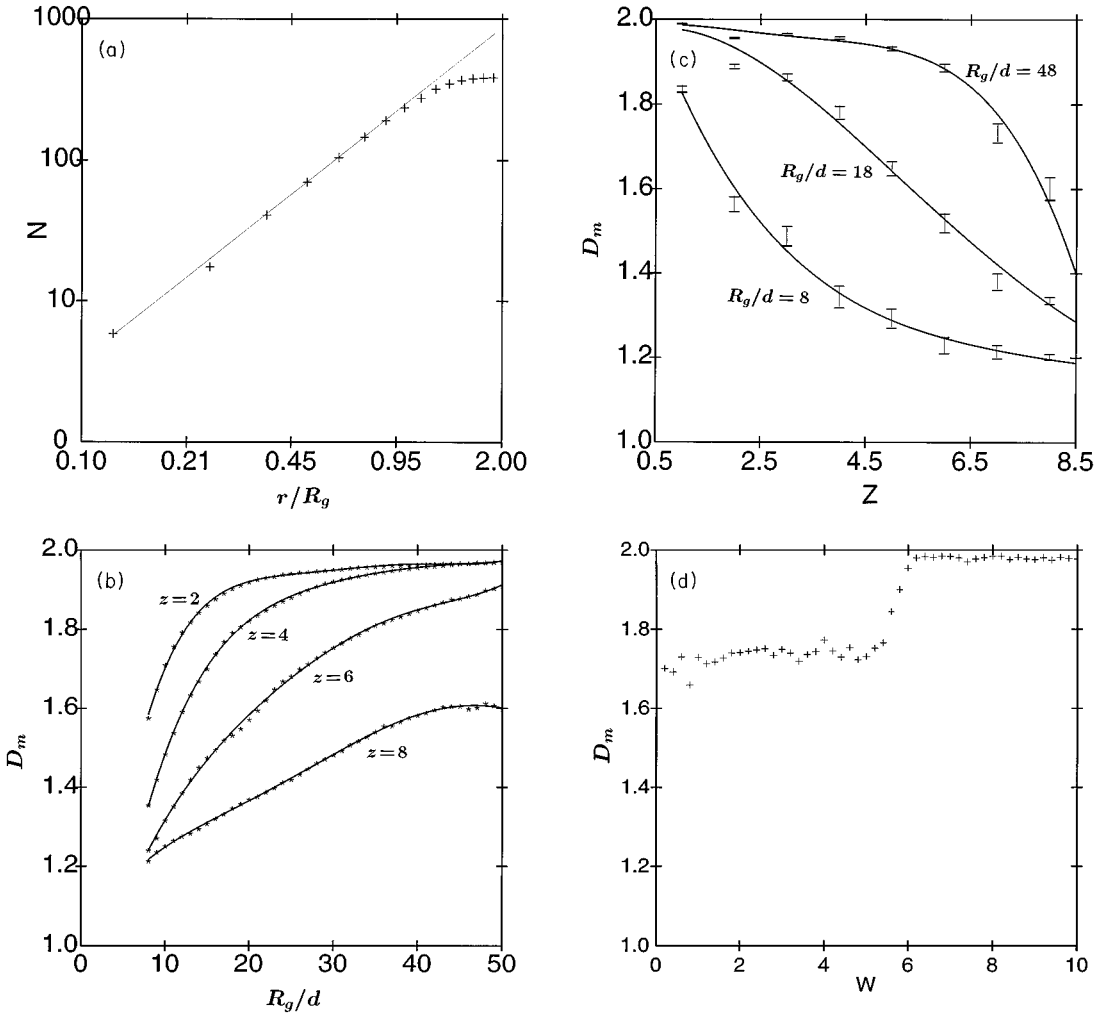

FIG. 4. (a) The number of cells N belonging to a magnetic domain located within a radius r from the nucleation site. The numerical data were obtained for a domain of the resolved radius of gyration $R_g/d=13$, where d is the separation of the hexagonal cells, using $z=2$, $w=4$, $\ln(k)=30$. (b) The mass fractal dimension D_m (averaged over a statistically independent ensemble of 100 magnetic domains) as a function of the resolved radius of gyration R_g/d. Results are presented for $w=2$ and different values for z. (c) The mass fractal dimension D_m as a function of the constant of demagnetizing strength z. The data were obtained using $w=2$, $\ln(k)=30$, three different radii of gyration averaging over an ensemble of 100 domains. (d) The mass fractal dimension as a function of the parameter w that is a measure of the domain-wall energy. The data were obtained using $z=3$, $R_g/d=12$, and averaging over 100 magnetic domains.

The perimeter-area relation [Eq. (27)] is satisfied in our model during the entire growth process, provided that the domains do not coalesce, as the linear dependence of $\ln(L)$ on $\ln(A)$ in Fig. 5(a) suggests.

A fractal geometry is usually observed when the laws that determine the growth process are deterministic, but there is disorder in material parameters.[42] If the system is homogeneous, a fractal geometry may still be observed provided that the growth process is stochastic. For instance, in diffusion-limited aggregation,[43] the growth process is controlled in effect by the geometry of space. In the present model, the growth of the perimeter of the magnetic domains is a similar example of stochastic growth in a film of homogeneous magnetic properties. In this respect, it is not surprising that the domain boundary is fractal. The wall dimension D_w appears, therefore to be a more useful fractal measure that the mass dimension D_m for the characterization of the domain regularity.

The dependence of the wall dimension D_w on the parameters z and w is shown in Figs. 5(b) and 5(c), respectively. The transition from a minimum value $D_w=1$ to the maximum value $D_w=2$ when the demagnetizing strength z is enhanced, shown in Fig. 5(b), indicates that the jaggedness of the domain boundary increases and is consistent with the computations in Ref. 10. The dependence on the wall energy w in Fig. 5(c) clearly has the opposite effect. The transitions observed in the value of D_w in Figs. 5(a) and 5(b) are not sharp, since there is always some diversity in the local magnetic environment along the perimeter of a magnetic domain of irregular shape.

Next we consider, the time dependence of the magnetization $M(t)$. The simplest treatment, based on Fatuzzo theory,[17] considers the nucleation at a rate R of circular domains of initial radius r_c, growing at constant velocity v and results in a time dependence given by

$$M(\tau)=M_s(2e^{g(\tau)}-1), \tag{28}$$

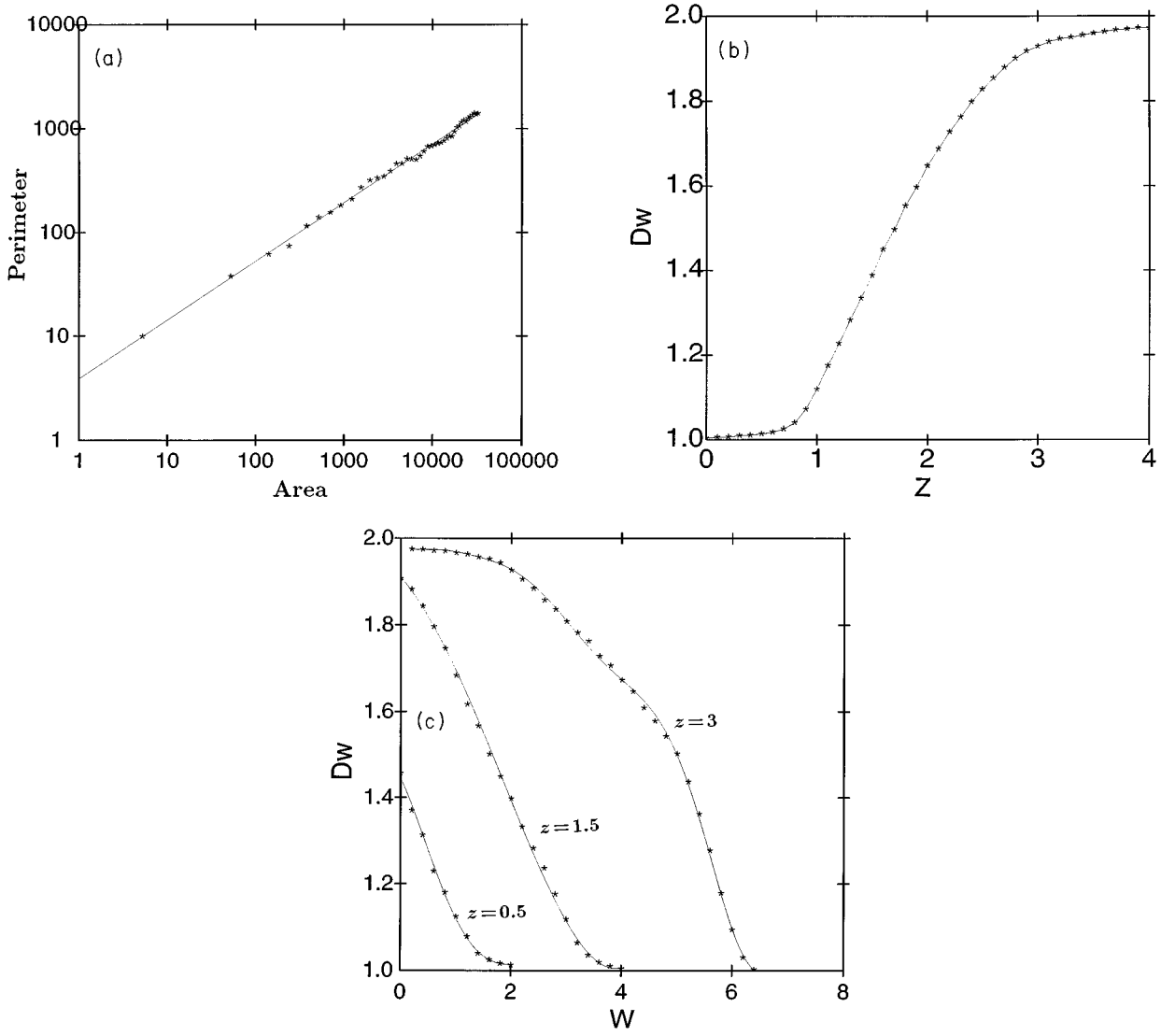

FIG. 5. (a) The perimeter-area relation for a magnetic domain. The data were obtained using $z=1$, $w=2$, and $\ln(k)=30$. The length of the perimeter is shown in units of the side $d/\sqrt{3}$ of a hexagonal cell (the length of the ruler). The area A is similarly normalized by the area $\sqrt{3}d^2/2$ occupied by a cell. (b) The fractal dimension of the domain wall D_w as a function of the demagnetizing field strength z. An average over 100 magnetic domains was taken using $w=2$ and $\ln(k)=30$. (c) The fractal dimension of the domain wall D_w as a function of the constant w that is a measure of the domain-wall energy. An average over 100 magnetic domains was taken using $\ln(k)=30$ and different values of demagnetizing strength z.

where $\tau=Rt$ and the function $g(\tau)$ is given by

$$g(\tau)=-2\kappa^2\left(1-(\tau+\kappa^{-1})+\frac{1}{2}(\tau+\kappa^{-1})^2-e^{-\tau}(1-\kappa^{-1})-\frac{1-\tau}{2\kappa^2}\right). \tag{29}$$

The shape of the time-dependence curves $M(t)$ is dependent on a single parameter $\kappa=v/Rr_c$. In principle, it is possible to compare the experimentally determined curves with the theory[16] and derive the value of κ that fits the data and provides a measure of the relative contribution of the nucleation and wall motion in the magnetic reversal. An alternative method of identification of the mechanism of magnetization reversal is to consider the curves involving the rate of change dM/dt. The variation of $d(M/M_s)/d\tau$ with τ, evaluated using the Fatuzzo theory [Eqs. (28) and (29)], is shown in Fig. 6(a). For nucleation-dominated reversal at low values of κ, the absolute magnitude of the rate $|dM/dt|$ exhibits a monotonic reduction. Conversely, for reversal dominated by domain-wall motion at large values of κ, a maximum value in the rate $|dM/dt|$ is observed that increases in magnitude at large values of κ. The dependence of the resolved rate $d(M/M_s)/dt$ on M/M_s is shown in Fig. 6(b). The dependence is linear for nucleation-dominated reversal, which is characterized by a single relaxation time $M=M_s(2e^{-t/\tau}-1)$. A maximum value of the rate $|dM/dt|$ occurs when $d^2M/dt^2=0$. Using Eqs. (28) and (29), it can be shown that the following condition must be satisfied:

$$2\kappa^2[\tau+(e^{-\tau}-1)(1-\kappa^{-1})+0.5\kappa^{-2}]^2+(1-\kappa^{-1})e^{-\tau}-1=0. \tag{30}$$

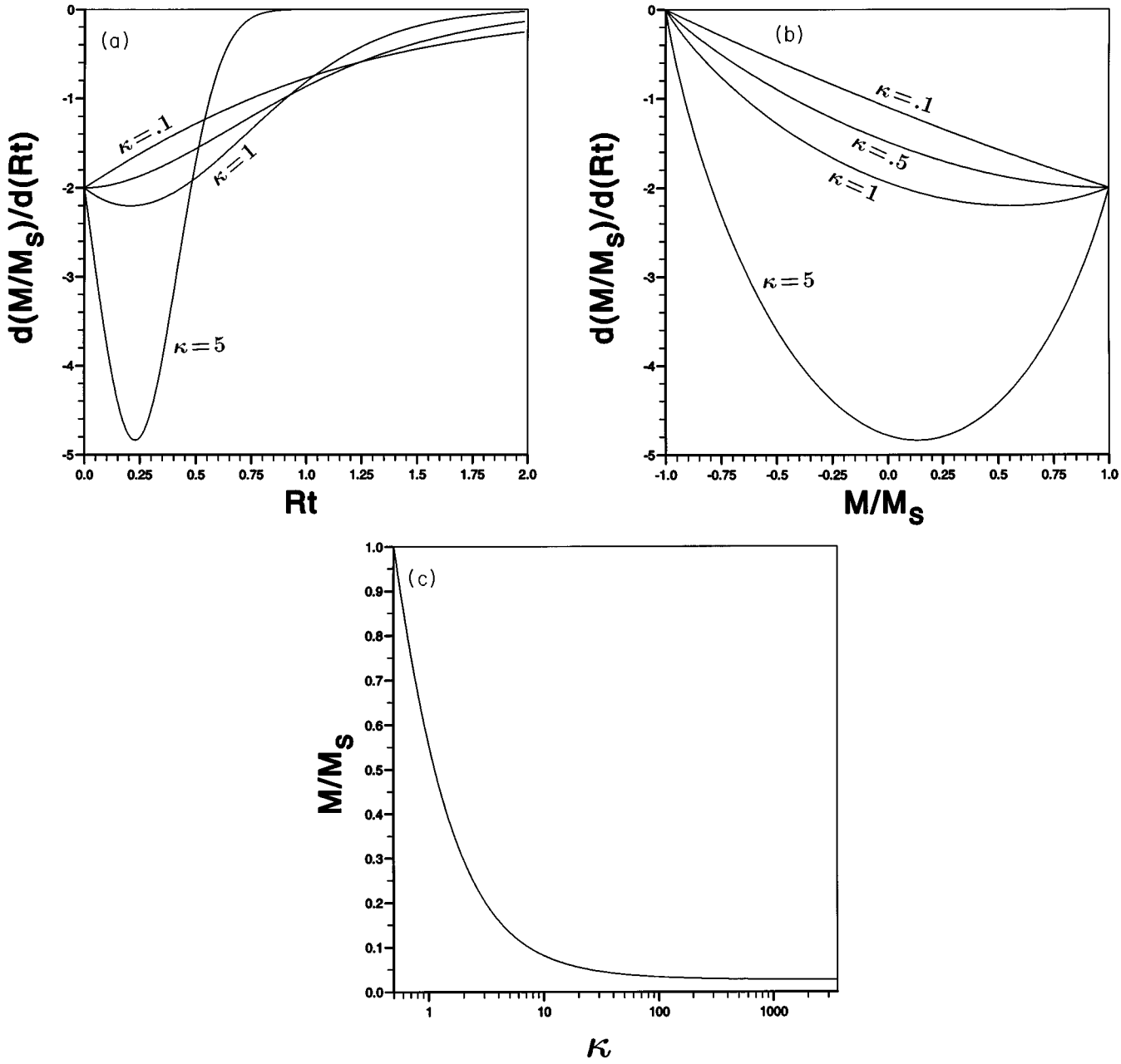

FIG. 6. (a) The time dependence of the rate of change of the magnetization according to the Fatuzzo model. Results are presented for κ=0.1,0.5,1,5. (b) The dependence of the rate of change of the magnetization on M/M_s according to the Fatuzzo model. Results are presented for κ=0.1,0.5,1,5. (c) The resolved magnetization M/M_s when the rate of magnetization reversal dM/dt attains the maximum value as a function of κ according to the Fatuzzo model.

A maximum value occurs for $\kappa>0.5$ at some value of the magnetization that is shown in Fig. 6(c) as a function of κ. The peak is displaced to lower values of the magnetization as κ increases, and in the limit $\kappa\rightarrow\infty$ it can be shown using $M(\tau)/M_s=2\exp(-\kappa^2\tau^3/3)-1$ (Ref. 17) that the condition $d^2M/dt^2=0$ is satisfied when $M/M_s=2e^{-2/3}-1$.

Fatuzzo's theory does not consider the demagnetization forces that result in the growth of fractal domain structures. dM/dt vs M plots obtained using the Monte Carlo model are shown in Fig. 7(a) for the case of continuous nucleation and in Figs. 7(b) and 7(c) for the case of reversal by wall motion. The monotonic reduction of the rate dM/dt in Fig. 7(a), the maximum of the rate in Figs. 7(b) and 7(c), and the enhancement of the maximum rate at large k are all consistent with the Fatuzzo theory. There are some important differences, however, that are attributed to the presence of the demagnetizing field.

In the case of reversal by continuous nucleation [Fig. 7(a)], the dependence of the rate dM/dt on M is nonlinear and, in addition, the magnetization freezes before complete reversal has been achieved. The demagnetizing field induces an effective dispersion in relaxation times that is also responsible for the shearing in the hysteresis loops [Fig. 3(a)]. A gradual reduction of the gradient $d(dM/dt)/dM$ is also evident in Figs. 7(b) and 7(c) and is in marked contrast [Fig. 6(b)] to the prediction of the Fatuzzo theory.

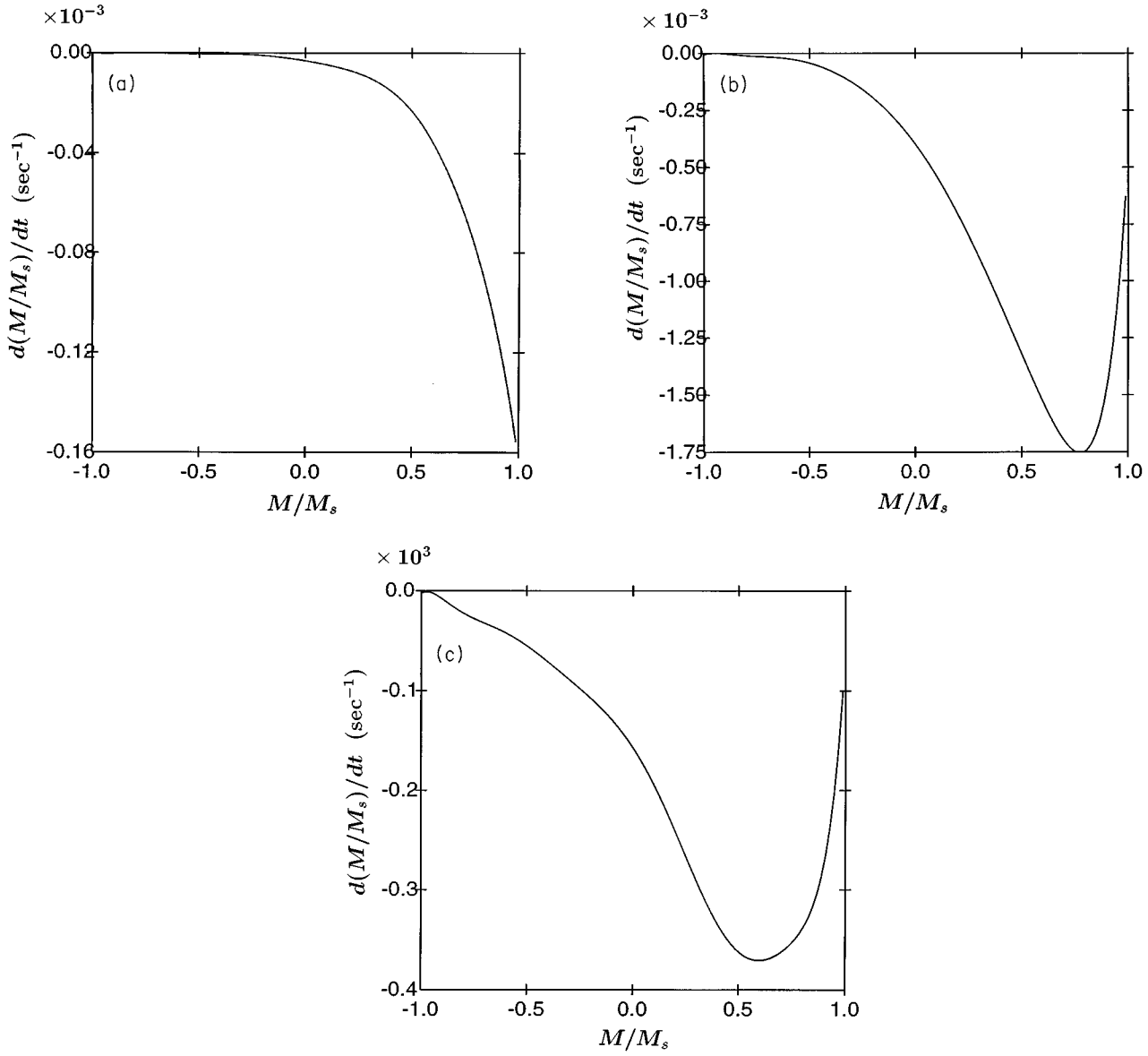

FIG. 7. The dependence of the rate of change of the magnetization on M/M_s using the Monte Carlo model. The results were obtained using $z=w=0.5$, $\ln(k)=0$ (a), $\ln(k)=5$ (b), and $\ln(k)=20$ (c). The instantaneous reversal in Eq. (9) was assumed to occur in 10^{-9} sec.

When the parameter k is allowed to increase, the peak in the rate dM/dt occurs at lower values of M, as expected by Fatuzzo theory [Fig. 6(c)]; the shift, however, is small, and the value $M/M_s=2e^{-2/3}-1$ is never reached. The demagnetizing field, by enhancing the energy barrier of thermoactivated wall motion, imposes a limitation on the rapid growth of the domains, during the initial stage that follows the nucleation process.

V. CONCLUSIONS

A Monte Carlo model of the thermoactivated magnetic reversal in thin films of RE-TM alloys has been developed that simulates the magnetic reversal mechanisms that are observed experimentally: reversal by continuous nucleation, nucleation followed by the growth of magnetic domains and dendritic growth by successive branching in the domain-wall motion. The magnetic reversal mechanism was found to depend in general on two factors. First, in accordance with the Fatuzzo theory, it is dependent on the difference in the intrinsic energy barriers of nucleation and domain-wall motion. For example, if the coercivities of nucleation and domain-wall motion are of the same magnitude, the magnetic reversal occurs by continuous nucleation; otherwise the preferred mechanism is by thermoactivated domain-wall motion. Second, it is also dependent on the relative balance of the demagnetizing and domain-wall energy, in agreement with previous theoretical and experimental work. When the demagnetizing forces are enhanced in magnitude in the simulations, the domain growth becomes rather abruptly dendritic by the formation of a maze-type pattern within the domain boundary. The observed maze-type pattern is rather uniform in thickness throughout the area enclosed by the domain boundary. The model does not predict the intermediate case of a small number of regions of unreversed magnetization in the interior of the domain, which is frequently

observed experimentally. The main reason appears to be the absence in the present model of a dispersion in intrinsic energy barriers for domain-wall motion.

The dendritic growth of the magnetic domains can be characterized by calculation of the mass fractal dimension D_m. The domain structures are not strictly fractal, since the dimension D_m increases during the growth process, i.e., the porosity of the magnetic domains is gradually reduced. In contrast, the domain perimeter is a fractal curve, and the fractal dimension D_w that describes the jaggedness of the domain wall is invariant during the growth process and constitutes, therefore, a good fractal measure of the domain regularity. It does not constitute, however, a measure of the domain shape that is related to, but not determined by, the ratio c in Eq. (27).

The demagnetizing field may result in shearing of the hysteresis loop. The amount of shearing appears to be dependent on the availability of space for domain expansion. The effects of the demagnetizing field on the time dependence of the magnetization under constant external field conditions were identified by comparison with the Fatuzzo theory, which ignores such effects. The Monte Carlo simulations indicate that in the presence of a finite demagnetizing field, the maximum value of the rate dM/dt occurs always early in the reversal process. This result is in disagreement with the prediction of the Fatuzzo model. Since the Fatuzzo model is often used to characterize the relative balance between thermoactivated nucleation and domain-wall motion in magneto-optic media, further work is necessary to determine the limitations of that approach.

The Monte Carlo results describe satisfactorily the domain structures observed in magneto-optic recording media other than RE-TM thin films, for example, amorphous multilayers such as Co/Pt (Ref. 37) and Dy/Fe (Ref. 24). A detailed study, however, should consider the magnetization reversal of individual layers. The model may also be useful for the description of ultrathin ferromagnetic films such as Au/Co/Au sandwiches.[27,28]

ACKNOWLEDGMENTS

The authors acknowledge the financial support of the Science and Engineering Research Council. We are indebted to Dr. S. D. Brown, Dr. P. Haycock, Professor J. N. Chapman, and Professor J. Ferré for helpful discussions.

[1] P. Hansen and H. Heitmann, IEEE Trans. Magn. **MAG-25**, 4390 (1989).
[2] M. H. Kryder, in *Applied Magnetism, NATO Advanced Study Institute Series E: Applied Sciences*, edited by R. Gerber, C. D. Wright, and G. Asti (Kluwer Academic, New York, 1994), p. 80.
[3] H. Fu, R. Giles, and M. Mansuripur, Comput. Phys. **8**, 80 (1994).
[4] M. Mansuripur, R. Giles, and G. Patterson, J. Appl. Phys. **69**, 4844 (1991).
[5] K. Ohashi, H. Takagi, S. Tsunashima, S. Uchiyama, and T. Fujii, J. Appl. Phys. **50**, 1611 (1979).
[6] K. Ohashi, H. Tsuji, S. Tsunashima, and S. Uchiyama, Jpn. J. Appl. Phys. **17**, 1333 (1980).
[7] T. G. Pokhil, B. S. Vvedensky, and E. N. Nikolaev (unpublished).
[8] T. G. Pokhil, B. S. Vvedensky, and E. N. Nikolaev, Mater. Sci. Forum **62–64**, 619 (1990).
[9] T. G. Pokhil and E. N. Nikolaev, IEEE Trans. Magn. **MAG-29**, 2536 (1993).
[10] G. V. Sayko, A. K. Zvezdin, T. G. Pokhil, B. S. Vvedensky, and E. N. Nikolaev, IEEE Trans. Magn. **MAG-28**, 2931 (1992).
[11] T. Thomson, K. O'Grady, C. M. Perlov, and R. W. Chantrell, IEEE Trans. Magn. **MAG-28**, 2518 (1992).
[12] T. Thomson, K. O'Grady, S. Brown, P. W. Haycock, and E. W. Williams, IEEE Trans. Magn. **MAG-28**, 2515 (1992).
[13] S. D. Brown, R. Street, R. W. Chantrell, and P. W. Haycock, J. Appl. Phys. (to be published).
[14] P. Bernstein and C. Gueugnon, J. Appl. Phys. **57**, 3601 (1985).
[15] F. Rio, P. Bernstein, and M. Labrune, IEEE Trans. Magn. **MAG-23**, 2266 (1987).
[16] M. Labrune, S. Andrieu, F. Rio, and P. Bernstein, J, Magn. Magn. Mater. **80**, 211 (1989).
[17] E. Fatuzzo, Phys. Rev. **127**, 1999 (1962).
[18] B. E. Bernacki and M. Mansuripur, J. Appl. Phys. **69**, 4960 (1991).
[19] B. E. Bernacki, T. Wu, and M. Mansuripur, J. Appl. Phys. **73**, 6838 (1993).
[20] A. A. Thiele, Bell Syst. Technol. J. **48**, 3287 (1969).
[21] H. D. Shieh and M. H. Kryder, J. Appl. Phys. **61**, 1108 (1987).
[22] K. Binder, *Monte Carlo Methods in Statistical Physics*, (Springer, Berlin, 1979), p. 33.
[23] A. Lyberatos, R. W. Chantrell, and A. Hoare, IEEE Trans. Magn. **MAG-26**, 222 (1990).
[24] R. D. Kirby, J. X. Shen, R. J. Hardy, and D. J. Sellmyer, Phys. Rev. B **49**, 10 810 (1994).
[25] J. Feder, *Fractals* (Plenum, New York, 1988), p. 11.
[26] F. D. Stacey, Aust. J. Phys. **13**, 599 (1960).
[27] A. Kirilyuk, J. Ferré, J. Pommier, and D. Renard, J, Magn. Magn. Mater. **121**, 536 (1993).
[28] G. Bayreuther, P. Bruno, G. Lugert, and C. Turtur, Phys. Rev. B **40**, 7399 (1989).
[29] P. Gaunt, J. Appl. Phys. **59**, 4129 (1986).
[30] A. Lyberatos, J. Appl. Phys. **75**, 5704 (1994).
[31] A. Kirilyuk, J. Ferré, and D. Renard, Europhys. Lett. **24**, 403 (1993).
[32] M. E. Schabes, Ph.D. thesis, University of California, San Diego, 1989.
[33] L. Néel, Ann. Geophys. **5**, 99 (1949).
[34] P. Gaunt, J. Appl. Phys. **48**, 3470 (1977).
[35] C. Kooy and U. Enz, Philips Res. Rep. **15**, 7 (1960).
[36] T. Thomson, Ph.D. thesis, University of Wales, 1993.
[37] J. X. Shen, R. D. Kirby, K. Wierman, Z. S. Shan, D. J. Sellmyer, and T. Suzuki, J. Appl. Phys. **73**, 6418 (1993).
[38] T. Suzuki, H. Notarys, D. C. Dobbertin, C.-J. Lin, D. Well, D. C. Miller, and G. Gorman, IEEE Trans. Magn. **MAG-28**, 2754 (1992).
[39] B. B. Mandelbrot, *The Fractal Geometry of Nature* (Freeman, New York, 1983).
[40] J. Feder, *Fractals* (Ref. 25).
[41] L. F. Richardson, Gen. Syst. Yearbook **6**, 139 (1961).
[42] J. D. Chen and D. Wilkinson, Phys. Rev. Lett. **55**, 1892 (1985).
[43] T. A. Witten and L. M. Sander, Phys. Rev. B **27**, 5686 (1983).